

Optimized kinematic dynamos

J. J. Love and David Gubbins

Department of Earth Sciences, The University of Leeds, Leeds LS2 9JT, UK

Accepted 1995 October 2. Received 1995 September 18; in original form 1995 February 21

SUMMARY

A numerical optimization approach is introduced to the subject of dynamo theory. Conventional kinematic dynamo studies treat the induction equation as an eigenvalue problem by choosing a candidate velocity field and solving for a marginally stable solution of magnetic field and critical magnetic Reynolds number. The conventional approach has told us something about dynamo action and magnetic field morphology for specific velocities, but the arbitrary choice of fluid flow is a hit-or-miss affair; not all velocities sustain dynamo action, and of those that do, few yield mathematically tractable solutions. As a result, progress has been slow. Here we adopt a new approach, a non-linear numerical variational approach, which allows us to solve the induction equation simultaneously for both the magnetic field and the velocity field. The induction equation is discretized following the Bullard–Gellman formalism and the resulting algebraic equations solved by an iterative, globally convergent, Newton–Raphson method. The particular choice of optimization constraints allows one to design a dynamo which satisfies certain conditions; in this paper we minimize a linear combination of the kinetic energy (magnetic Reynolds number) and a smoothness norm on the magnetic field to produce efficient (low magnetic Reynolds number) well-converged (smooth magnetic field) solutions. We illustrate the optimization method by designing two dynamos based on a Kumar–Roberts velocity parametrization; a specific choice of the velocity parameters, KR, sustains a 3-D kinematic model of the geodynamo. Compared with KR, one of our new models, LG1, is designed to have a higher magnetic Reynolds number but smoother magnetic field, and the other, LG2, a lower magnetic Reynolds number and somewhat rougher magnetic field. We suggest that dynamo efficiency, defined by the magnetic Reynolds number, is achieved through reduced differential rotation and a favourable spatial distribution of the helicity. These examples demonstrate the value of the optimization method as a tool for exploring dynamo action with geophysically realistic flows. It can be extended to the dynamic dynamo problem and, by changing the constraints, be used to design dynamos with good numerical convergence, which match the observed geomagnetic surface field morphology and which place useful quantitative constraints on the physical nature of the geodynamo.

Key words: geomagnetism, inverse problem, numerical techniques.

1 INTRODUCTION

A dynamo converts mechanical energy into magnetic energy. For the geomagnetic field, convective motion in the Earth's liquid iron outer core provides the requisite mechanical energy; advective amplification of the magnetic field offsets the destructive effect of diffusion. Modelling of the geodynamo usually takes the form of a deterministic numerical experiment. In a *dynamic* experiment one investigates magnetic induction by a convecting fluid and the forces necessary to sustain the fluid motion as determined by the full set of magnetohydrodynamic

equations, namely the induction equation, the Navier–Stokes equation of motion, and an equation describing the convective energy source, either thermal or compositional buoyancy. In a *kinematic* analysis, such as that conducted here, one investigates the types of fluid motions which sustain dynamo action, regardless of the forces necessary to maintain the flows, by solving only the magnetic induction equation,

$$\partial_t \hat{\mathbf{B}} = R_m \nabla \times (\mathbf{u} \times \hat{\mathbf{B}}) + \nabla^2 \hat{\mathbf{B}}, \quad (1)$$

where $\hat{\mathbf{B}} = \mathbf{B}e^{pt}$ denotes the time-dependent magnetic field, p

is the complex growth rate, and \mathbf{u} is the dimensionless fluid velocity. The magnetic Reynolds number is $R_m = \mu\sigma Uc$, where U and c are typical core velocities and length-scales, respectively (see Table 1), and $(\mu\sigma)^{-1}$ is the magnetic diffusivity. R_m gives a measure of the effectiveness by which fluid motion acts to amplify the magnetic field compared to the rate, $\tau_d = \mu\sigma c^2$, at which the magnetic field decays due to electrical resistance. If $\Re_e[p(R_m)] \geq 0$ then we have dynamo action, otherwise the magnetic field decays. For the marginal state, $\Re_e[p(R_m^c)] = 0$, advective amplification and diffusive decay are in balance and if $\Im_m(p) = 0$ then the magnetic field is steady, otherwise it is oscillatory with frequency $\Im_m(p)/(2\pi)$. R_m^c is called the *critical* magnetic Reynolds number. It is desirable, from a geophysical standpoint, to find dynamos which have magnetic Reynolds numbers like that of the core, $R_m = O(100)$.

At first glance the kinematic dynamo problem seems enticingly simple: for a given velocity field, \mathbf{u} , eq. (1) is linear and a solution can be sought by treating it as an eigenvalue problem, where \mathbf{B} is the eigenvector. This bold, if straightforward, approach for the case of a fluid sphere was attempted by Bullard & Gellman (1954). By expanding both the velocity field and magnetic field in terms of spherical harmonics and radial grid points, Bullard & Gellman reduced the induction equation to a large matrix equation, amenable to standard numerical techniques. The apparent simplicity of this approach is beguiling, however. In fact, the numerical treatment of the 3-D spherical kinematic dynamo problem has proven to be remarkably difficult, and apparent solutions have subsequently been shown to be spurious, as was the case for the velocity field chosen by Bullard & Gellman.

The difficulty arises because advection tends to twist and tangle the magnetic field, thereby producing a field which is spatially complex, having energy at small length-scales (high spherical harmonic degree), and making it difficult to represent numerically. Diffusion reduces the magnetic energy at short length-scales, but only to a limited extent because the very nature of dynamo action is a non-trivial balance between advective amplification and diffusive destruction of the magnetic field. However, for many velocity fields, the generation of short-length-scale magnetic energy is sufficient to prevent a low-degree truncation of the spherical harmonic expansion of the magnetic field. In fact, because of limitations of computer power, it is commonly impossible to consider a harmonic expansion large enough to ensure numerical convergence; in such cases it is impossible to tell if the velocity field supports dynamo action, since a balance between advection and diffusion may occur at spherical harmonic degrees well beyond the level of truncation. Hence, one of the main problems vexing kinematic dynamo theory is numerical convergence.

Seeking to avoid the obvious difficulties presented by eq. (1), Steenbeck, Krause & Rädler (1966), motivated by the early work of Parker (1955), developed the theory of mean-field electrodynamics. In their theory an average is taken over the

short length-scales and rapid fluctuations of turbulence to obtain a mean induction equation,

$$\partial_t \bar{\mathbf{B}} = R_m \nabla \times (\alpha \bar{\mathbf{B}} + \bar{\mathbf{u}} \times \bar{\mathbf{B}}) + \nabla^2 \bar{\mathbf{B}}, \quad (2)$$

where the overbar denotes a spatial and temporal average. The new term in this equation, $\alpha \bar{\mathbf{B}}$, represents the so-called α -effect, where α is linearly related to the mean helicity,

$$\bar{h} = \overline{\mathbf{u} \cdot \nabla \times \mathbf{u}} \quad (3)$$

(Moffatt 1978). A related dynamo theory, developed shortly before that of Steenbeck, Krause & Rädler, is the nearly axisymmetric dynamo of Braginsky (1964). With a spherical geodynamo in mind, Braginsky constructed a nearly axisymmetric dynamo with an α -effect arising from azimuthal averaging that is valid in the limit $R_m \rightarrow \infty$. Mean-field electrodynamics and model-Z allow for a convenient quantitative expression of Parker's (1955) $\alpha\omega$ mechanism. The ω -effect, supported by differential rotation, causes a pre-existing, primarily dipolar, poloidal field to be wound about the rotational axis, thereby producing a quadrupolar toroidal field. Fluid upwelling, with the appropriate amount of helicity, lifts and twists the toroidal field, thereby producing loops of poloidal field by the α -effect. These loops of poloidal field coalesce and reinforce the pre-existing dipolar field, thus completing the dynamo cycle. The saving grace of mean-field electrodynamics and model-Z is that they circumvent Cowling's theorem. This allows for dynamos which, in the mean, are axisymmetric, thus permitting numerically convergent solutions, simpler than those obtained for the fully 3-D induction equation (1).

There is no doubt that we have learned more about the dynamo process from studies of the $\alpha\omega$ equations than from direct attacks on the 3-D induction equation. However, the stringent assumption that a net α -effect could arise from very short-length-scale, chaotic motion of turbulence is of questionable applicability to the Earth's core; the energetics are probably insufficient to sustain sufficiently turbulent motion with the Coriolis and the Lorentz forces acting together to produce large-scale fluid motion. Specifically, for model-Z (Braginsky 1964) the necessary energy is geophysically excessive; the fluid flow is too fast ($\sim 4.7 \times 10^{-3} \text{ m s}^{-1}$) and the toroidal field is too strong ($\sim 74 \text{ mT}$), consequences of model-Z's requisite large magnetic Reynolds numbers. Moreover, the geomagnetic field exhibits significant deviations from axisymmetry, a property which is explicitly excluded from model-Z. Thus, despite attendant difficulties, any complete theory of the geodynamo must consider the 3-D induction equation (1).

The few 3-D kinematic dynamos that do sustain well-behaved magnetic fields have been found, with great effort, by trial and error. It is this arbitrary search for solutions that is perhaps the most unsatisfactory aspect of a kinematic dynamo analysis and is largely responsible for its difficulty: some velocity fields act as dynamos and some do not. Of those that do, few yield numerically tractable solutions and fewer still

Table 1. Numerical values used in this analysis.

Symbol		Value
μ	Magnetic permeability	$4\pi \times 10^{-7} \text{ H/m}$
c	Radius of the core	$3.5 \times 10^6 \text{ m}$
U	Typical fluid velocity in the core	$\sim 10^{-4} \text{ m/s}$
B_r	Typical strength of the radial field at the CMB	$\sim 3 \times 10^{-4} \text{ T}$
σ	Electrical conductivity of the core	$\sim 3 \times 10^5 \text{ S/m}$

sustain fields that bear any resemblance to the observed geomagnetic field. Moreover, a physically reasonable R_m cannot be imposed as it is an intrinsic parameter of the fluid flow.

In this paper we introduce a means of searching systematically for suitable velocity fields. Rather than imposing the velocity field and treating the induction equation as a linear eigenvalue problem, in our non-linear approach the velocity field and magnetic field are both treated as unknown variables. Solutions to the induction equation are obtained, subject to constraints on the magnetic and velocity fields, using standard optimization techniques. We are guided by the success of geophysical inverse theory: we call the conventional approach to the dynamo, where the magnetic field is determined after imposing a velocity field, the *forward* method, and the new approach, where both the magnetic and velocity fields are solved subject to prescribed constraints, the *optimization* or *inverse* method.

We are not the first to adopt this approach: Cowling (1934) proved his celebrated anti-dynamo theorem by an inverse method. Constraining the magnetic field to be axisymmetric, Cowling attempted to solve for both the velocity and magnetic field. Since no solutions exist, he proved that axisymmetric magnetic fields cannot be sustained by dynamo action. However, dynamo solutions can be found by adopting constraints that are less restrictive than those of Cowling: by choosing different constraints we can design a range of solutions to answer specific questions. For example, in this paper we obtain numerically convergent kinematic dynamos with physically plausible magnetic Reynolds numbers by minimizing a weighted combination of the kinetic energy and a smoothness norm on the magnetic field.

2 THE FORWARD PROBLEM

2.1 The Bullard–Gellman formalism

The behaviour of the geomagnetic field is complex: over historical times the field at the core surface has exhibited static, rapidly drifting and oscillating features (Bloxham & Gubbins 1985), and of course the magnetic field occasionally undergoes a reversal. But recent analysis of palaeomagnetic data (Gubbins & Kelly 1993) reveals that much of the field can, over very long time-scales, be characterized as steady. For this reason, and for the sake of simplicity, we seek only steady dynamo solutions, although time-dependent solutions have also been extensively studied. By prescribing \mathbf{u} in eq. (1), we have the generalized eigenvalue problem,

$$\nabla \times (\mathbf{u} \times \mathbf{B}) = -R_m^{-1} \nabla^2 \mathbf{B}, \quad (4)$$

where \mathbf{B} is the eigenvector and $-R_m^{-1}$ is the eigenvalue. It is this steady problem that Bullard & Gellman (1954) attempted to solve by the spectral method.

As an approximation to the Earth, let us consider a conducting fluid sphere of unit radius, $r = 1$, representing the core, surrounded by a solid electrical insulator, representing the mantle. It is natural, then, to use spherical coordinates (r, θ, ϕ) where \mathbf{r} is the position vector and $\hat{\mathbf{r}}$ is the unit vector pointing outwards from the centre of the sphere. Since the magnetic field is solenoidal,

$$\nabla \cdot \mathbf{B} = 0, \quad (5)$$

we can represent the magnetic field in spherical coordinates by its toroidal and poloidal ingredients,

$$\mathbf{B} = \mathbf{T} + \mathbf{S} = \sum_{l,m} \mathbf{B}_l^m = \sum_{l,m} (\mathbf{T}_l^m + \mathbf{S}_l^m). \quad (6)$$

The toroidal and poloidal vectors, $\mathbf{T}(r, \theta, \phi)$ and $\mathbf{S}(r, \theta, \phi)$, are defined as

$$\mathbf{T} = \nabla \times (\mathcal{T} \hat{\mathbf{r}}), \quad \mathbf{S} = \nabla \times \nabla \times (\mathcal{S} \hat{\mathbf{r}}), \quad (7)$$

where the toroidal and poloidal scalar functions are $\mathcal{T}(r, \theta, \phi)$ and $\mathcal{S}(r, \theta, \phi)$. The individual vector components $\mathbf{B}_l^m(r, \theta, \phi)$, $\mathbf{T}_l^m(r, \theta, \phi)$ and $\mathbf{S}_l^m(r, \theta, \phi)$ are

$$\begin{aligned} \mathbf{B}_l^m &= \mathbf{T}_l^m + \mathbf{S}_l^m, & \mathbf{T}_l^m &= \nabla \times (T_l^m Y_l^m \hat{\mathbf{r}}), \\ \mathbf{S}_l^m &= \nabla \times \nabla \times (S_l^m Y_l^m \hat{\mathbf{r}}), \end{aligned} \quad (8)$$

where $T_l^m(r)$ and $S_l^m(r)$ are the toroidal and poloidal radial functions. The spherical harmonics, $Y_l^m(\theta, \phi)$, are

$$Y_l^{m(c,s)} = P_l^m \begin{cases} \cos m\phi \\ \sin m\phi \end{cases}, \quad (9)$$

where $P_l^m(\cos \theta)$ is a Schmidt-normalized associated Legendre function. Thus,

$$\oint_{4\pi} Y_{l_1}^{m_1} Y_{l_2}^{m_2} d\Omega = \frac{4\pi}{2l_1 + 1} \delta_{l_1}^{l_2} \delta_{m_1}^{m_2}, \quad (10)$$

where the integration is over all solid angles $d\Omega$. For simplicity we shall assume that the fluid in the core is incompressible,

$$\nabla \cdot \mathbf{u} = 0, \quad (11)$$

and thus, like the magnetic field, the velocity field may be represented by its toroidal and poloidal ingredients,

$$\mathbf{u} = \mathbf{t} + \mathbf{s} = \sum_{l,m} (\mathbf{t}_l^m + \mathbf{s}_l^m). \quad (12)$$

Spherical harmonic expansions for the velocity field are similar to those for the magnetic field.

Ampère's law in pre-Maxwell form relates the electric current to the magnetic field,

$$\nabla \times \mathbf{B} = \mathbf{J}, \quad (13)$$

where \mathbf{J} is the dimensionless current density. Thus,

$$\nabla \times \mathbf{T} = \nabla \times \nabla \times (\mathcal{T} \hat{\mathbf{r}}), \quad \nabla \times \mathbf{S} = \nabla \times [(-\nabla^2 \mathcal{S}) \hat{\mathbf{r}}], \quad (14)$$

which shows that toroidal fields are sustained by poloidal currents and vice versa. Insofar as the mantle is an insulator, the potential field in the mantle is a special case of a poloidal field and is sustained by electric currents in the core. On the other hand, a toroidal field, being entirely non-potential, is trapped within a conductor; consequently toroidal magnetic fields vanish at and above the core's surface. In the mantle, then,

$$\mathbf{B} = -\nabla\Phi. \quad (15)$$

If we require that the magnetic field be entirely internally sustained, in other words that there are no external sources, then the potential is described by the expansion

$$\Phi = \sum_{l,m} a_l^m r^{-(l+1)} Y_l^m. \quad (16)$$

The magnetic field is continuous at the core's surface and must match onto a potential field; thus, after equating components,

we obtain the boundary conditions

$$T_l^m = 0, \quad \frac{\partial S_l^m}{\partial r} + \frac{1}{r} S_l^m = 0, \quad \text{at } r = 1. \quad (17)$$

At the origin regularity requires that

$$T_l^m = O(r^{l+1}), \quad S_l^m = O(r^{l+1}), \quad \text{at } r = 0. \quad (18)$$

If the magnetic field is non-zero and satisfies the steady induction equation, then enforcement of the boundary conditions (17) and (18) is tantamount to requiring dynamo action in the region $0 < r < 1$.

After substituting eqs (6) and (12) into eq. (4), Bullard & Gellman obtained the infinite set of ordinary differential equations

$$\sum_{\substack{l_2, m_2 \\ l_3, m_3}} F_{l_1}^{m_1}(t_{l_2}^{m_2}, s_{l_2}^{m_2}, T_{l_3}^{m_3}, S_{l_3}^{m_3}) = -R_m^{-1} [r^2 \partial_r^2 T_{l_1}^{m_1} - l_1(l_1 + 1) T_{l_1}^{m_1}], \quad (19)$$

$$\sum_{\substack{l_2, m_2 \\ l_3, m_3}} G_{l_1}^{m_1}(t_{l_2}^{m_2}, s_{l_2}^{m_2}, T_{l_3}^{m_3}, S_{l_3}^{m_3}) = -R_m^{-1} [r^2 \partial_r^2 S_{l_1}^{m_1} - l_1(l_1 + 1) S_{l_1}^{m_1}], \quad (20)$$

where $F_{l_1}^{m_1}$ and $G_{l_1}^{m_1}$, which depend on Gaunt and Elsasser integrals, are complicated bilinear functions of the velocity harmonic coefficients (t_l^m, s_l^m) and magnetic field harmonic coefficients (T_l^m, S_l^m), as well as their first and second radial derivatives. To find a solution to eqs (19) and (20), Bullard & Gellman divided the range $0 \leq r \leq 1$ into M equal parts. After approximating the radial derivatives by finite differences and truncating the spherical harmonic expressions they obtained a coupled set of algebraic equations, which, with enforcement of the boundary conditions, (17) and (18), can be written in the form

$$\mathbf{A}: (\mathbf{u} \otimes \mathbf{b}) = -R_m^{-1} \mathbf{D} \cdot \mathbf{b}, \quad (21)$$

which should be compared with eq. (4). In this notation, the magnetic field is represented throughout the volume of the core by the vector \mathbf{b} , where an individual element b_i is a spherical harmonic coefficient for either the toroidal or poloidal magnetic field ingredient at a given radial grid point. Likewise, \mathbf{u} represents the velocity field at all points throughout the volume of the core, individual elements being u_i . The advection tensor \mathbf{A} is of third order, $\mathbf{u} \otimes \mathbf{b}$ is a dyad (see e.g. Malvern 1969), and the contraction $\sum_{j,k} A_{ijk} u_j b_k$ is the i th element of the vector $\mathbf{A}: (\mathbf{u} \otimes \mathbf{b})$. Diffusion is represented by the matrix \mathbf{D} , and the product $\mathbf{D} \cdot \mathbf{b}$ is a vector.

The reduction of the induction equation to the form of eq. (21) makes it amenable to standard numerical methods. With the specification of \mathbf{u} , the equations are linear in \mathbf{b} and inverse iteration can be used to locate both the eigenvalue $-R_m^{-1}$ and the eigenvector \mathbf{b} , provided \mathbf{u} sustains dynamo action and truncation of the spherical harmonic and radial grid-point expansions is not made so prematurely that numerical convergence cannot be ensured. The usual procedure then is to truncate the radial representation at M grid points and the spherical harmonic expansion at degree and order N , locate the eigenvalue and eigenvector, then increase both M and N and again locate the eigenvalue and eigenvector. If after successive increases in the level of truncation both the eigenvalue and eigenvector are unchanged to within a numerically small and tolerable amount, then the result may be judged convergent and we conclude that we have a solution to the

induction equation (Gubbins 1973). Otherwise, if successive increments of M or N give intolerably different results, no solution is obtained and the velocity field is deemed incapable of supporting numerically convergent magnetic fields. In practice, checking for numerical convergence can require a substantial amount of computer power and for this reason, as we discuss in the next section, some apparently valid results have later been shown to be illusive.

2.2 Previous investigations

The history of 3-D kinematic dynamo theory has been one of frustration. Bullard & Gellman (1954), initiating the subject, investigated the velocity

$$\mathbf{u} = t_1^0 + \varepsilon s_2^{2c}, \quad (22)$$

where ε is an adjustable parameter and the radial dependence of $t_1^0(r)$ and $s_2^{2c}(r)$ is fixed. This velocity field was an attempt to simulate the motion in the core; differential rotation, t_1^0 , inspired by the observed westward drift of the Earth's magnetic field and laboratory simulations of rotating convective systems, is thought to be the dominant motion in the core, with some poloidal overturn—they chose s_2^{2c} —being both a necessary ingredient for dynamo action and a consequence of internally driven convection. Initially, it appeared that Bullard & Gellman found a convergent stationary dynamo, but, unfortunately, subsequent checks with higher levels of truncation (Gibson & Roberts 1969) showed that eq. (22) does not sustain numerically convergent solutions. It appears, at least for their choice of radial dependence, that dynamo action is not possible for this velocity field. Indeed, Braginsky (1964) showed that flows such as (22), which possess a plane of mirror symmetry containing the rotation axis, do not behave as dynamos in the limit $R_m \rightarrow \infty$. Lilley (1970) removed the offending symmetry by considering the flow

$$\mathbf{u} = t_1^0 + s_2^{2s} + s_2^{2c}, \quad (23)$$

reporting that this led to convergent solutions. Once again, however, more rigorous checks (Gubbins 1973) showed that convergence was not attained for Lilley's choice of radial functions, although later investigations (Hutcherson 1990; Nakajima & Kono 1991; Hutcherson & Gubbins 1990) showed that modification of the radial functions in the Lilley dynamo can yield converged solutions.

Gubbins (1973) and Pekeris, Accad & Shkoller (1973) introduced several flows which, as subsequent analyses have confirmed, sustain numerically convergent magnetic fields. Although these studies convincingly demonstrated 3-D dynamo action for the first time, none of their flows, nor the magnetic fields that they support, possess the symmetries characteristic of the core. Gubbins & Bloxham (1987) have pointed out a nearly stationary, four-fold symmetry in the historical magnetic field and Gubbins & Zhang (1993) have summarized the symmetries thought to characterize the geodynamo. In short, it is desirable, at least from a geophysical standpoint, to find dynamos with magnetic fields antisymmetric under reflection through the equatorial plane, E^A , sustained by flows which are mirror symmetric about the equatorial plane, E^S , as emphasized by Busse (1983). Moreover, analyses of historical and modern measurements of the geomagnetic field made over the last 400 years (Bloxham, Gubbins & Jackson 1989) and palaeomagnetic data over geological time-

scales (Gubbins & Kelly 1993; Johnson & Constable 1995) indicate that the geodynamo can be characterized as symmetric, at least roughly, under rotation about the geographic axis by an angle of π radians, a symmetry denoted as P_2^S . In addition to lending a bit of geophysical realism, enforcement of the $E^A P_2^S$ symmetry, which is just one of the many symmetries consistent with the induction equation, has the benefit of reducing by a factor of four the number of terms in the spherical harmonic expansions, thereby substantially reducing the size of the matrix equation (21).

Kumar & Roberts (1975) found numerically convergent magnetic fields possessing the $E^A P_2^S$ symmetry using the flow

$$\mathbf{u} = \varepsilon_0 \mathbf{t}_1^0 + \varepsilon_1 \mathbf{s}_2^0 + \varepsilon_2 \mathbf{s}_2^{2s} + \varepsilon_3 \mathbf{s}_2^{2c}, \quad (24)$$

which itself has the requisite E^S symmetry. The defining scalars are

$$t_1^0 = r^2(1 - r^2), \quad (25)$$

$$s_2^0 = r^6(1 - r^2)^3, \quad (26)$$

$$s_2^{2s} = r^4(1 - r^2)^2 \cos(pr), \quad (27)$$

$$s_2^{2c} = r^4(1 - r^2)^2 \sin(pr), \quad (28)$$

where $\{\varepsilon_0, \varepsilon_1, \varepsilon_2, \varepsilon_3\}$, and p are parameters. Aside from satisfying the desired symmetries, this flow, like others used in kinematic dynamo theory, is in detail arbitrary, although in a geophysical context it is qualitatively appropriate. The toroidal motion, \mathbf{t}_1^0 , induces an ω -effect, creating toroidal magnetic field from poloidal field, and the sectoral harmonics, \mathbf{s}_2^{2s} and \mathbf{s}_2^{2c} , contribute to convective overturning. This flow also contains a meridional circulation, \mathbf{s}_2^0 , which Roberts (1972) found to promote steady solutions in $\alpha\omega$ -dynamos. The parameter p in eqs (27) and (28) determines the number of convective cells in the radial direction; throughout this analysis we shall take $p = 3\pi$. The velocity components (25)–(28) are shown in Fig. 1.

Kumar & Roberts found that their dynamo is sensitive to the choice of $\{\varepsilon_0, \varepsilon_1, \varepsilon_2, \varepsilon_3\}$, reporting a particularly well-converged solution for the combination $\{1.000, 0.030, 0.040, 0.040\}$. These values give a dynamo with $R_m \approx 3850$. A more appropriate definition of R_m uses a volume average to scale the velocity field,

$$U = \langle \mathbf{u} \rangle, \quad (29)$$

where we define

$$\langle \dots \rangle^2 = V^{-1} \int_C \|\dots\|^2 dV, \quad (30)$$

and where C denotes integration over the volume of the core, V . With this scaling this model, hereafter referred to as KR, has the velocity parameters $\{4.410, 0.132, 0.176, 0.176\}$, with dynamo action occurring for $R_m \approx 900$. Unfortunately, this R_m is uncomfortably large in a geophysical context. However, we must emphasize that this was not a concern for Kumar & Roberts, since they were more interested in checking the

validity of Braginsky's dynamo where $R_m \rightarrow \infty$. The properties of the models are given in Table 2.

From our standpoint, the main advantage of the Kumar & Roberts velocity field (24) is its ability to sustain a numerically convergent steady magnetic field, and for this reason we have selected it to illustrate our optimization procedure. Hutcheson & Gubbins (1994) have remarked that (24) sustains a surface magnetic field that possesses four high-flux patches coincident with fluid downwelling, which bear some resemblance to the Earth's magnetic field at the core–mantle boundary: two in the Northern Hemisphere of one polarity and, since the dynamo field has E^A symmetry, two in the Southern Hemisphere of the opposite polarity. Such fortuitous geophysical verisimilitude is, from our perspective, satisfying.

3 THE OPTIMIZATION PROBLEM

Since a spatially complex magnetic field is difficult to describe mathematically by a finite expansion of basis functions, we seek velocity fields which sustain spatially simple, and therefore, it is hoped, numerically convergent magnetic fields with geophysically plausible magnetic Reynolds numbers. One way of promoting numerical convergence is to seek those dynamos which minimize some measure of the spatial complexity of the magnetic field. For example, we can seek the dynamo which minimizes $\langle \nabla^2 \mathbf{B} \rangle$, for some non-trivial magnetic field strength. Of course $\nabla^2 \mathbf{B}$ is related to R_m , and it might be thought that dynamos with a minimum R_m could be similar to those with a minimum $\langle \nabla^2 \mathbf{B} \rangle$. But this is certainly an oversimplification, since R_m is a constant scalar whilst the vector $\nabla^2 \mathbf{B}$ is spatially variable, and they are really only related to each other through the rather complicated advective term of the induction equation. From a geophysical standpoint, though, it is desirable to obtain a relatively small magnetic Reynolds number appropriate for the Earth's core, $R_m = O(100)$.

Thus, to study the relationship between spatial complexity of the magnetic field and magnetic Reynolds number, it seems sensible to find those solutions that minimize some weighted combination of both R_m and $\langle \nabla^2 \mathbf{B} \rangle$. Such an objective can be attained by numerical optimization. To that end, we pose a variational problem, seeking a minimum of the non-linear non-dimensional functional

$$\begin{aligned} \Psi(R_m \mathbf{u}, \mathbf{B}, \mathbf{q}, \gamma) = & v_1 \langle R_m \mathbf{u} \rangle^2 + v_2 \langle \nabla^2 \mathbf{B} \rangle^2 \\ & + \int_C \mathbf{q} \cdot [\nabla \times (R_m \mathbf{u} \times \mathbf{B}) + \nabla^2 \mathbf{B}] dV \\ & + \gamma [\langle \mathbf{B} \rangle^2 - 1], \end{aligned} \quad (31)$$

where the components of the vector function \mathbf{q} and the scalar γ are Lagrange multipliers. Note that we have combined the magnetic Reynolds number and the velocity field in the augmented variable $R_m \mathbf{u}$, and if we define R_m so that

$$\langle \mathbf{u} \rangle = 1, \quad (32)$$

Table 2. Properties of the three dynamo models.

Model	ε_0	ε_1	ε_2	ε_3	R_m	$\langle \mathbf{B} \rangle^2 = 1$					$\ \mathbf{B}_{SD}\ = 1$	$\langle h \rangle = 1$	Geophysical quantities		
						$\langle \nabla^2 \mathbf{B} \rangle^2$	$\langle \mathbf{J} \rangle^2$	$\langle \mathbf{T} \rangle^2$	$\langle \mathbf{S} \rangle^2$	$\langle \mathbf{B}_{AS} \rangle^2$			$\langle \mathbf{B}_{NA} \rangle^2$	$\langle \mathbf{B} \rangle^2$	$ h _N$
KR	4.400	0.132	0.176	0.176	900	6 880	63.4	0.994	0.006	0.989	0.011	16 000	0.21	37.9	2.81
LG1	4.410	0.039	0.144	0.159	1400	5 090	56.7	0.997	0.003	0.991	0.009	32 700	0.12	54.2	5.14
LG2	3.686	0.689	0.770	0.752	144	13 000	73.4	0.873	0.127	0.909	0.091	324	2.78	5.4	0.07

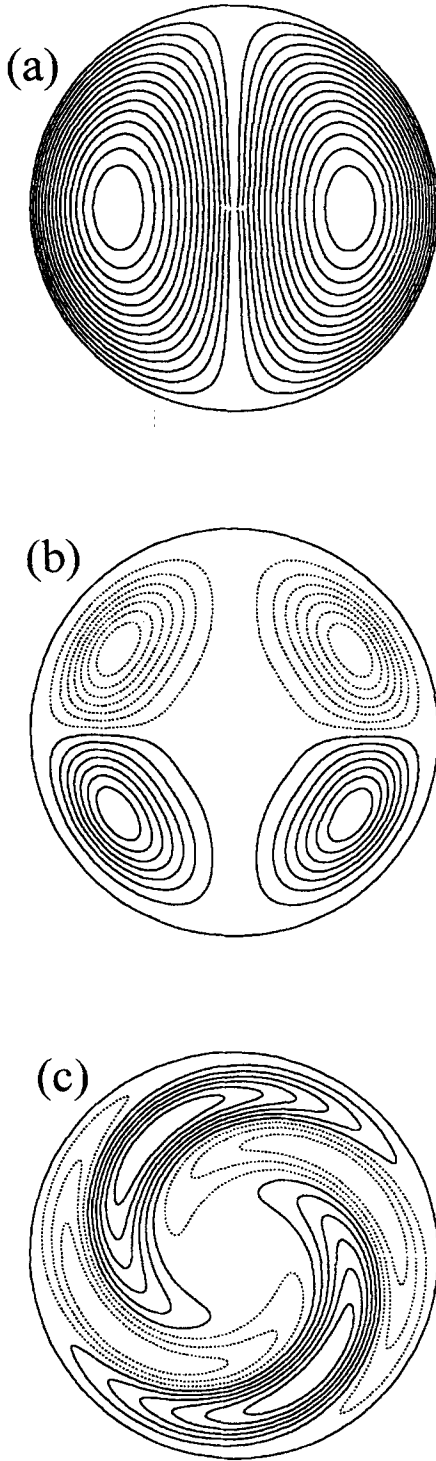


Figure 1. Velocity components: (a) contours of toroidal flow t_1^0 in meridional section; (b) streamlines of the poloidal flow component s_2^0 in meridional section; (c) streamlines of the poloidal flow component $s_2^c + s_2^s$ in equatorial section.

then

$$R_m = \langle R_m \mathbf{u} \rangle. \quad (33)$$

Thus, after effecting the minimum of Ψ , by adjusting the variables $\{R_m \mathbf{u}, \mathbf{B}, \mathbf{q}, \gamma\}$ in the manner described below, we obtain the magnetic Reynolds number R_m , the velocity field \mathbf{u}

and the magnetic field \mathbf{B} , which are consistent with dynamo action and which minimize a combination of R_m and $\langle \nabla^2 \mathbf{B} \rangle$, the relative weighting being determined by the adjustable parameters v_1 and v_2 . The last term in eq. (31) is a non-triviality constraint, designed to ensure that our normalization,

$$\langle \mathbf{B} \rangle = 1, \quad (34)$$

holds; we are free to choose a normalization, such as this one, on account of the linearity in \mathbf{B} of the induction equation.

Following the treatment of Bullard & Gellman (1954), we express the velocity and magnetic fields in terms of their poloidal and toroidal scalar functions, and then express these scalar functions in terms of spherical harmonic expansions and radial grid points. $R_m \mathbf{u}$, \mathbf{B} and \mathbf{q} are then completely described throughout the volume of the core by vectors of model coefficients \mathbf{u}_R , \mathbf{b} and \mathbf{q} respectively. After enforcing the boundary conditions, the functional (31) can be expressed in matrix notation as

$$\Psi(\mathbf{x}) = v_1 \mathbf{u}_R \cdot \mathbf{N} \cdot \mathbf{u}_R + v_2 \mathbf{b} \cdot \mathbf{M} \cdot \mathbf{b} + \mathbf{q} \cdot \mathbf{A} : (\mathbf{u}_R \otimes \mathbf{b}) + \mathbf{q} \cdot \mathbf{D} \cdot \mathbf{b} + \gamma \mathbf{b} \cdot \mathbf{L} \cdot \mathbf{b} - \gamma, \quad (35)$$

where the vector \mathbf{x} is defined as

$$\mathbf{x} = \begin{bmatrix} \mathbf{u}_R \\ \mathbf{b} \\ \mathbf{q} \\ \gamma \end{bmatrix}, \quad (36)$$

and where we note that \mathbf{q} is a vector of the same length as \mathbf{b} . A minimum of Ψ is obtained where the set of non-linear algebraic equations $\mathbf{f}(\mathbf{x})$ equals zero,

$$\mathbf{f}(\mathbf{x}) = \partial_{\mathbf{x}} \Psi = 0, \quad (37)$$

where

$$\mathbf{f}(\mathbf{x}) = \begin{bmatrix} 2v_1 \mathbf{N} \cdot \mathbf{u}_R + \mathbf{A}^{T^{qu}} : (\mathbf{q} \otimes \mathbf{b}) \\ 2v_2 \mathbf{M} \cdot \mathbf{b} + \mathbf{A}^{T^{qb}} : (\mathbf{u}_R \otimes \mathbf{q}) + \mathbf{D}^T \cdot \mathbf{q} + 2\gamma \mathbf{L} \cdot \mathbf{b} \\ \mathbf{A} : (\mathbf{u}_R \otimes \mathbf{b}) + \mathbf{D} \cdot \mathbf{b} \\ \mathbf{b} \cdot \mathbf{L} \cdot \mathbf{b} - 1 \end{bmatrix}, \quad (38)$$

and where, for example, T^{qu} denotes the transpose with respect to \mathbf{q} and \mathbf{u}_R . Notice that the third row in the column vector (38) is the induction equation and the fourth row is the normalization condition; thus at $\mathbf{f}(\mathbf{x})=0$ both the induction equation and the normalization condition are satisfied.

We solve $\mathbf{f}(\mathbf{x})=0$ using an iterative globally convergent Newton-Raphson technique; see, for example, Dennis & Schnabel (1983). Starting from an initial guess \mathbf{x}_0 , we expand \mathbf{f} in a Taylor series,

$$\mathbf{f}(\mathbf{x}_0 + \delta \mathbf{x}) = \mathbf{f}(\mathbf{x}_0) + \mathbf{J} \cdot \delta \mathbf{x} + O(\delta \mathbf{x}^2), \quad (39)$$

where the Jacobian is

$$\mathbf{J} = \begin{bmatrix} 2v_1 \mathbf{N} & \mathbf{A}^{T^{qu}} \cdot \mathbf{q}_0 & \mathbf{A}^{T^{quT^{qb}}} \cdot \mathbf{b}_0 & 0 \\ \mathbf{A}^{T^{qbT^{qu}}} \cdot \mathbf{q}_0 & 2v_2 \mathbf{M} + 2\gamma_0 \mathbf{L} & \mathbf{A}^{T^{qb}} \cdot \mathbf{u}_{R0} + \mathbf{D}^T & 2\mathbf{L} \cdot \mathbf{b}_0 \\ \mathbf{A}^{T^{bu}} \cdot \mathbf{b}_0 & \mathbf{A} \cdot \mathbf{u}_{R0} + \mathbf{D} & 0 & 0 \\ 0 & 2\mathbf{b}_0 \cdot \mathbf{L} & 0 & 0 \end{bmatrix}. \quad (40)$$

Taking $\mathbf{f}(\mathbf{x}_0 + \delta\mathbf{x}) = 0$, we obtain the set of linear equations

$$\mathbf{J} \cdot \delta\mathbf{x} = -\mathbf{f}(\mathbf{x}_0), \quad (41)$$

which we solve for $\delta\mathbf{x}$ by using *LU* decomposition, taking full advantage of the sparsity of \mathbf{J} to save on computer memory. Since the full Newton step $\delta\mathbf{x}$ may move us outside the quadratic approximation of (39), we obtain the new vector \mathbf{x}_1 by moving possibly only partway along the direction $\delta\mathbf{x}$. Thus

$$\mathbf{x}_1 = \mathbf{x}_0 + \xi\delta\mathbf{x}, \quad 0 < \xi \leq 1, \quad (42)$$

where ξ is adjusted so that

$$\|\mathbf{f}(\mathbf{x}_1)\|^2 < \|\mathbf{f}(\mathbf{x}_0)\|^2, \quad (43)$$

thereby ensuring that \mathbf{x}_1 is always an improvement upon the initial guess \mathbf{x}_0 . Once we have \mathbf{x}_1 , we make the reassignment $\mathbf{x}_1 \rightarrow \mathbf{x}_0$ and repeat the process until some prescribed convergence criterion is satisfied.

In practice, we have found it useful to use a dynamo as an initial guess; in other words, we use a combination $\{R_m \mathbf{u}, \mathbf{B}\}$ which satisfies the induction equation. We use zero as the initial guess of the Lagrange multipliers. As with the forward problem, once we have the desired optimized solution, we must, for the given truncation level, check for numerical convergence. This is best done by fixing \mathbf{u} , then solving the eigenvalue problem (4) for different levels of truncation, as we would for an ordinary kinematic dynamo problem by the method described at the end of Section 2.1. The set $\{R_m \mathbf{u}, \mathbf{B}\}$ obtained by solving the eigenvalue problem should be the same as that obtained by optimization; such a comparison obviously functions as a useful test of the optimization code.

4 OPTIMIZING THE KUMAR & ROBERTS VELOCITY FIELD

4.1 Construction and comparison of models

Although a general parametrization of the velocity field is permissible in the above optimization procedure, in terms of spherical harmonic coefficients and radial grid points for example, here we limit ourselves to the four free velocity parameters of Kumar & Roberts in eq. (24). The vector describing the product of magnetic Reynolds number and velocity then takes the simple form

$$R_m \mathbf{u} = R_m (\varepsilon_0 \mathbf{t}_1^0 + \varepsilon_1 \mathbf{s}_2^0 + \varepsilon_2 \mathbf{s}_2^{2s} + \varepsilon_3 \mathbf{s}_2^{2c}), \quad (44)$$

so that

$$\mathbf{u}_R = \mathbf{u}_R (R_m \{\varepsilon_0, \varepsilon_1, \varepsilon_2, \varepsilon_r\}). \quad (45)$$

With this limited velocity field we have succeeded in locating a suite of dynamos, two of which we discuss here. The first model, designated LG1, was obtained by minimizing Ψ of eq. (31) for magnetic roughness, $\langle \nabla^2 \mathbf{B} \rangle$, by simply setting $v_1 = 0$, and v_2 equal to a small positive value. The second

model, LG2, was obtained by minimizing a combination of both R_m and $\langle \nabla^2 \mathbf{B} \rangle$. The details of both of these models are presented in Table 2. Following Gubbins (1973), and as we discussed at the end of Section 2.1, we check the convergence properties of these two models, along with those of KR, by comparing both the magnetic Reynolds number, Table 3, and the eigenfunctions, Fig. 2, for differing levels of truncation (M, N) . Fig. 2 may be compared with Fig. 2 of Hutchison & Gubbins (1994) for the KR model. Clearly, KR, LG1 and LG2 are all well-converged dynamos: substantial increases in the level of truncation do not significantly change either R_m or the eigenfunctions for $(M, N) \gtrsim (150, 10)$.

Table 2 illuminates some of the differences between the three dynamo models. Since we obtained LG1 by minimizing $\langle \nabla^2 \mathbf{B} \rangle$, after using KR as an initial guess, LG1 necessarily supports a smoother magnetic field than KR, whilst LG2, again on account of the type of minimization applied, has a smaller R_m than either KR or LG1. The average current density, $\langle \mathbf{J} \rangle$, for the unit normalization of the magnetic field (34), is least for LG1 and greatest for LG2. Other differences between the models are apparent when one compares the relative proportions of toroidal magnetic energy and poloidal magnetic energy, defined respectively as

$$\langle \mathbf{T} \rangle^2 = \sum_{l,m} \langle \mathbf{T}_l^m \rangle^2, \quad \langle \mathbf{S} \rangle^2 = \sum_{l,m} \langle \mathbf{S}_l^m \rangle^2, \quad (46)$$

or the relative proportions of axisymmetric energy with non-axisymmetric energy, defined respectively as

$$\langle \mathbf{B}_{AS} \rangle^2 = \sum_l \langle \mathbf{B}_l^0 \rangle^2, \quad \langle \mathbf{B}_{NA} \rangle^2 = \sum_{\substack{l,m \\ (m \neq 0)}} \langle \mathbf{B}_l^m \rangle^2. \quad (47)$$

Dynamos KR and LG1 have greater proportions of axisymmetric and toroidal magnetic energies than does LG2. This is consistent with the ω -effect; KR and LG1 have a greater proportion of their fluid motion, as measured by ε_0 , in the form of differential rotation than does LG2, and as a result the toroidal magnetic field, primarily the axisymmetric quadrupolar component, is proportionately stronger in KR and LG1 than in LG2. Conversely, LG2 has a greater proportion of non-axisymmetric and poloidal energies than do KR and LG1, a fact consistent with a greater proportion of convective motion in LG2, as measured by ε_2 and ε_3 , which causes a relative amplification of the non-axisymmetric poloidal field via the α -effect.

The magnetic energy for each model, given as a function of harmonic degree, is

$$\langle \mathbf{B}_l \rangle^2 = \sum_m \langle \mathbf{B}_l^m \rangle^2, \quad (48)$$

and is plotted in Fig. 3, where we have renormalized the magnetic field so that the dipole at the core surface is unity, $\|\mathbf{B}_{SD}\| = 1$. Since our dynamo models are numerically convergent, the magnetic energy decreases with increasing harmonic degree for all three models, the reddest spectrum being that of

Table 3. Comparison of magnetic Reynolds numbers for different levels of truncation (M, N) with unit normalization of the velocity field, $\langle \mathbf{u} \rangle = 1$. That the differences in R_m for the higher truncation levels are slight is indicative of numerically convergent solutions.

	(100,7)	(100,8)	(100,9)	(150,10)	(150,11)	(150,12)	(200,13)	(200,14)
KR	918.34	912.14	912.15	897.56	897.72	897.57	892.71	892.69
LG1	1459.78	1435.75	1440.73	1402.37	1402.44	1402.31	1390.30	1389.91
LG2	143.51	144.26	144.13	143.50	143.65	143.66	143.47	143.44

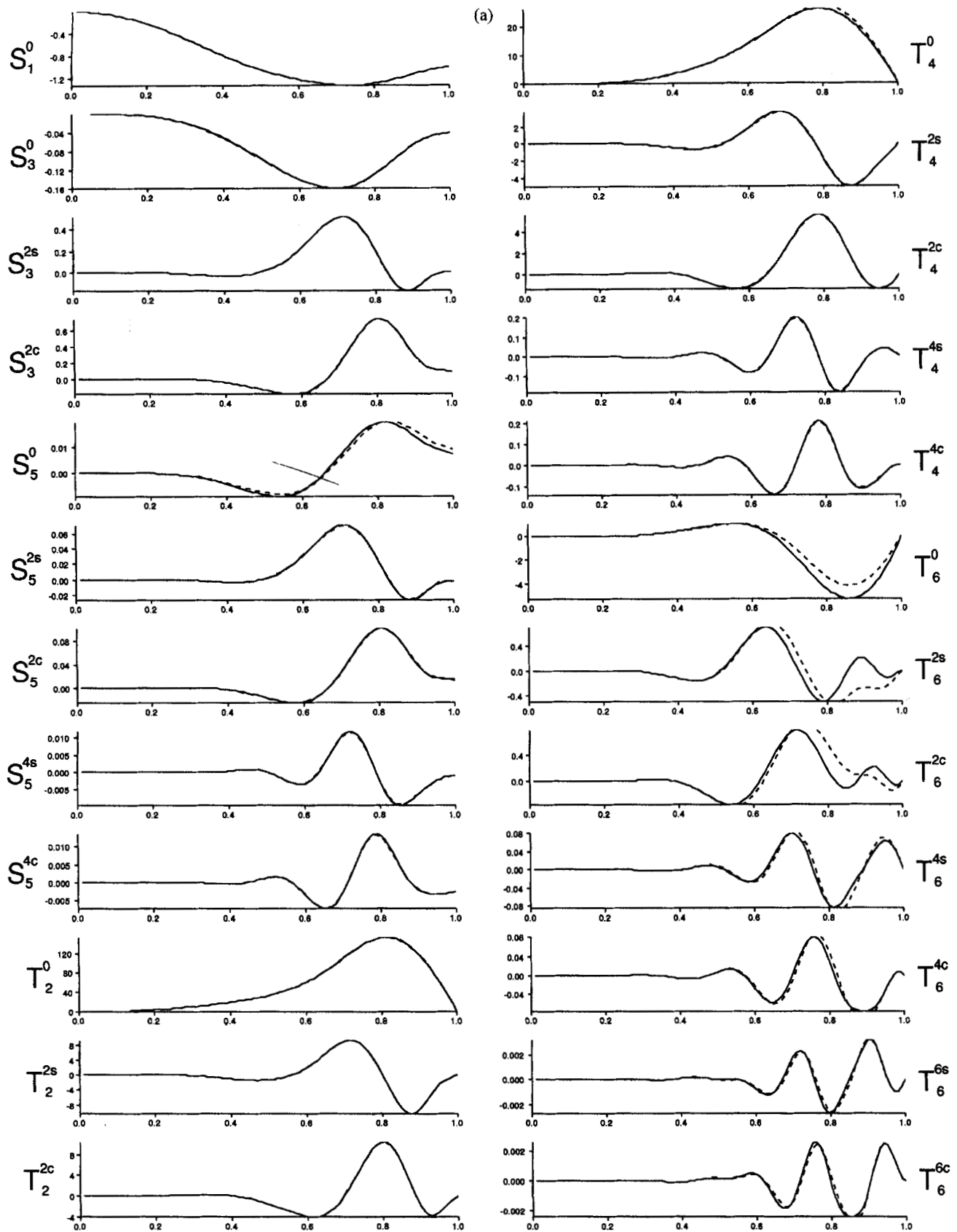


Figure 2. Comparison of radial functions for models LG1 (a) and LG2 (b) for different levels of truncation (M, N). The dashed lines represent the solution for truncation (100, 8) and the solid lines represent (100, 16). That the differences in the radial functions for different truncations is slight is indicative of numerically convergent solutions. Radial functions for the KR are given in Hutcheson & Gubbins (1994).

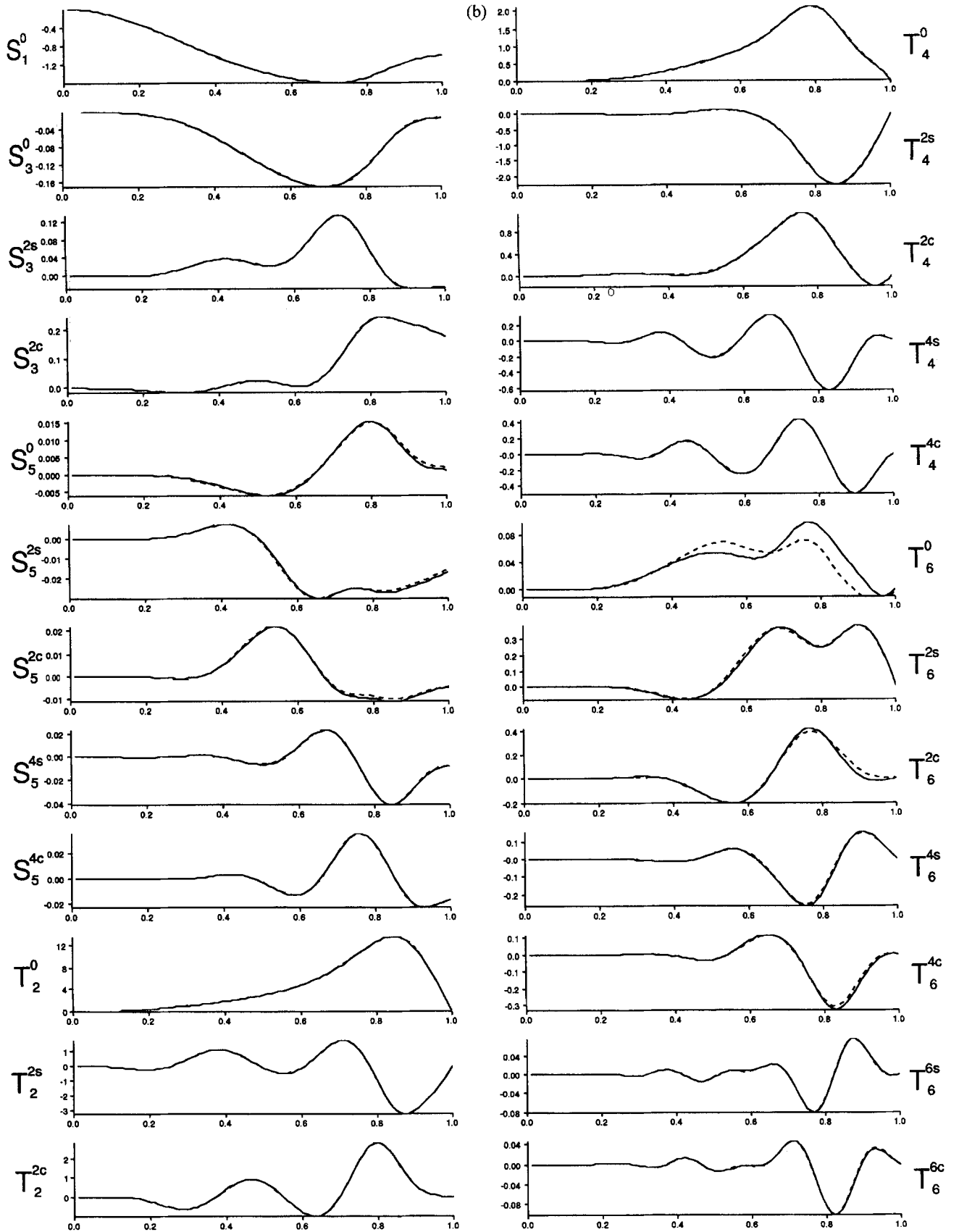


Figure 2. (Continued.)

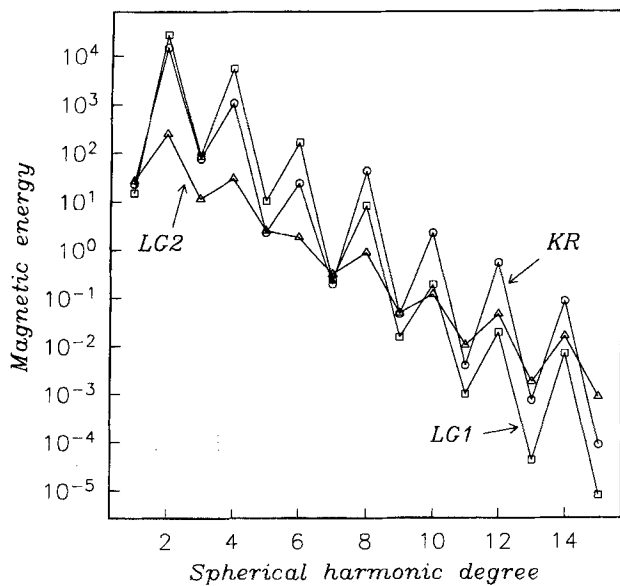


Figure 3. Magnetic energy spectrum, $\langle B_l \rangle^2$, for the original Kumar & Roberts (1975) dynamo model and the two optimized dynamos derived in this study. That the energies decrease with increasing harmonic degree is indicative of numerically convergent solutions. The sawtooth pattern is caused by the symmetry imposed on the solution. Large, axisymmetric toroidal harmonics have even degree and tend to dominate the spectrum for models KR and LG1.

LG1, the bluest that of LG2, a result consistent with the differences in $\langle \nabla^2 \mathbf{B} \rangle$. The differences in the spectra are manifest in plots of the magnetic fields. In Fig. 4(a) we show the ϕ -average of the poloidal field in meridional cross-section; all three models show little difference. The non-axisymmetric form

and greater spatial complexity, i.e. the blueness, of LG2 is apparent in Fig. 4(b), where we plot contours of B_θ in equatorial section. A similar observation can be made of B_ϕ ; in Fig. 5(a) we see little difference in the ϕ -averaged toroidal field, but the greater spatial complexity of LG2 is apparent in the unaveraged meridional sections, Figs 5(b) and 5(c).

The relatively slight overall differences between LG1 and KR reveal that Kumar & Roberts found a dynamo which very nearly minimizes the spatial roughness, $\langle \nabla^2 \mathbf{B} \rangle$, of the magnetic field. Indeed, LG1 is only slightly smoother than KR, but the important difference, of course, is that our dynamo models were constructed systematically, whilst KR was found with great effort after much trial and error. The utility of our optimization technique is illustrated further by the fact that we have been able to construct a dynamo, LG2, which has both a satisfactory degree of convergence and a geophysically plausible magnetic Reynolds number, $O(100)$.

Interestingly enough, despite significant differences in R_m , the poloidal fields sustained at the surface of the core, $r=1$, are qualitatively similar; see Fig. 6. The slight differences in the surface fields are caused by different proportions of meridional circulation and differential rotation. Of the three models, LG2 has the strongest gradients in flux at low latitudes, a result of larger meridional circulation, as measured by ϵ_1 , which sweeps flux towards the equator, and weaker differential rotation, as measured by ϵ_0 , which shears out poloidal flux at low latitudes.

4.2 Geophysical comparisons

Although we do not claim that our dynamo models reproduce the details of the geodynamo—indeed, our analysis is only kinematic—none the less it is useful to make a few geophysical

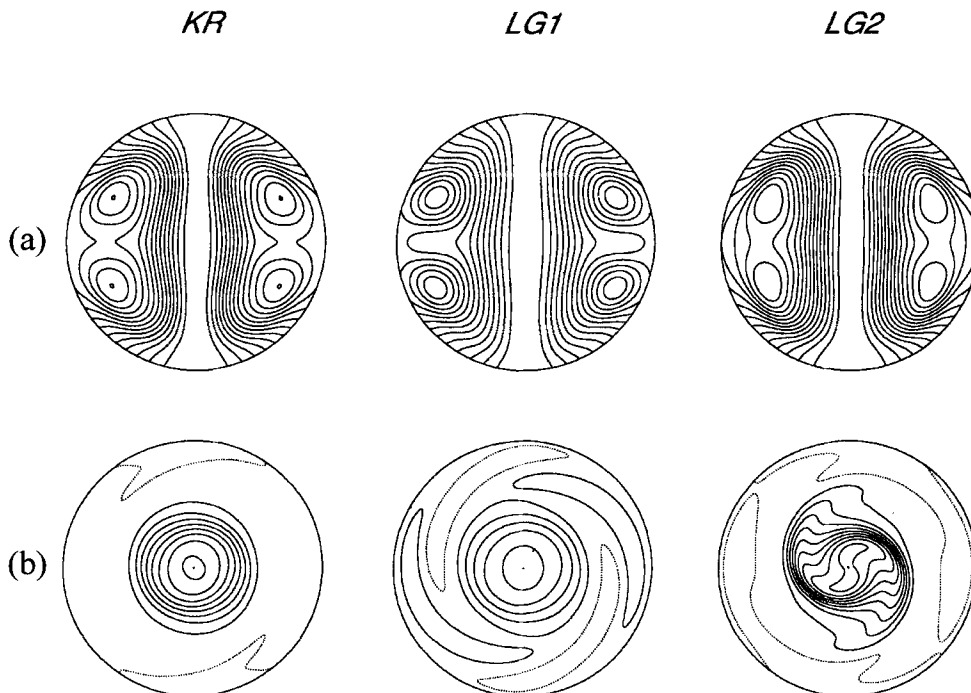


Figure 4. Poloidal magnetic fields for the three dynamo models with the field strength normalized so that the surface dipole is unity, $\|\mathbf{B}_{SD}\| = 1$. The contour intervals are all equal. (a) Azimuthal average of the poloidal field in a meridional plane. (b) B_θ in an equatorial section. Note the greater complexity of model LG2, which is not apparent in azimuthal average.

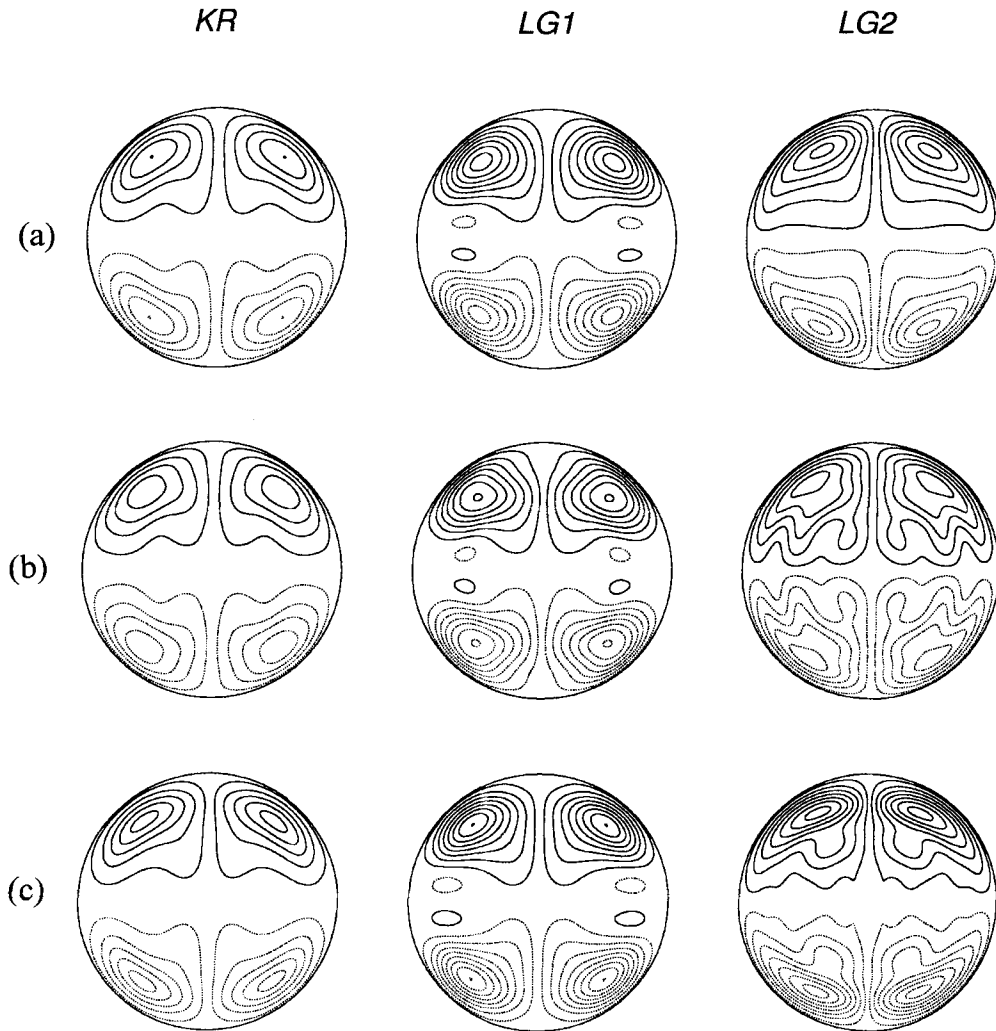


Figure 5. Toroidal magnetic fields for the three dynamo models with the field strength normalized so that the surface dipole is unity, $\|\mathbf{B}_{\text{SD}}\| = 1$. The contour intervals for KR and LG1 are equal and ten times larger than that for LG2. (a) Azimuthal average of the toroidal field in a meridian plane; (b) toroidal field in the meridian plane $\phi = 0$; (c) toroidal field in the meridian plane $\phi = 90^\circ$.

comparisons. If, for each model, we match the strength of the surface, $r = 1$, dipole with that at the core surface, ~ 0.3 mT, we obtain the corresponding average strengths of the magnetic fields in the model interiors; see Table 2. A very rough upper bound on the magnetic field strength for the core can be obtained assuming that the dynamics are governed by a balance between the Coriolis and Lorentz forces (Hide & Roberts 1979). Such a magnetostrophic balance occurs for a magnetic field strength of ~ 10 mT, a limit which is consistent with thermodynamic arguments (Gubbins, Masters & Jacobs 1979). Both KR and LG1 have average magnetic field strengths that might be considered somewhat excessive; on the other hand, LG2 certainly has a field strength acceptably below the magnetostrophic limit.

Another useful comparison is one of the ohmic dissipation, Q , of the dynamo models, Table 2. Of the observed surface heat flow, 4×10^{13} W (Sclater, Jaupart & Galson 1980), about three-quarters comes from radioactivity in the mantle (Stacey 1977); the remainder comes from a wide variety of sources, including radioactivity in the core, remnant heat of accretion, tidal dissipation, latent heat release, and ohmic dissipation in the core (Gubbins *et al.* 1979). Although a precise limit on the

amount of ohmic dissipation that contributes to the surface heat flow is not available, the ohmic dissipations of KR and LG1, calculated assuming a core conductivity of 3×10^5 S m $^{-1}$, are probably excessive, but the dissipation of LG2 is acceptable.

5 EFFICIENCY AND CONVERGENCE

Dynamo LG2 has a smaller magnetic Reynolds number than either KR or LG1, and in that sense is the most efficient of our three dynamo models. Some insight into the cause of this difference in efficiency may be gained by inspecting the spatial distribution of helicity. Since the helicity for (24) is E^A , a property qualitatively consistent with rotating convection (Moffatt 1978), following Nakajima & Kono (1991) we calculated the helicity averaged over the Northern Hemisphere,

$$|h|_N = 2V^{-1} \int_0^{2\pi} \int_0^{\pi/2} \int_0^1 hr^2 dr \sin \theta d\theta d\phi, \quad (49)$$

for each of the dynamo models. From Table 2 we notice that $|h|_N$ is greatest for LG2. Nakajima & Kono have suggested that velocities with larger $|h|_N$ support dynamo action with smaller R_m , and our results are consistent with their hypothesis.

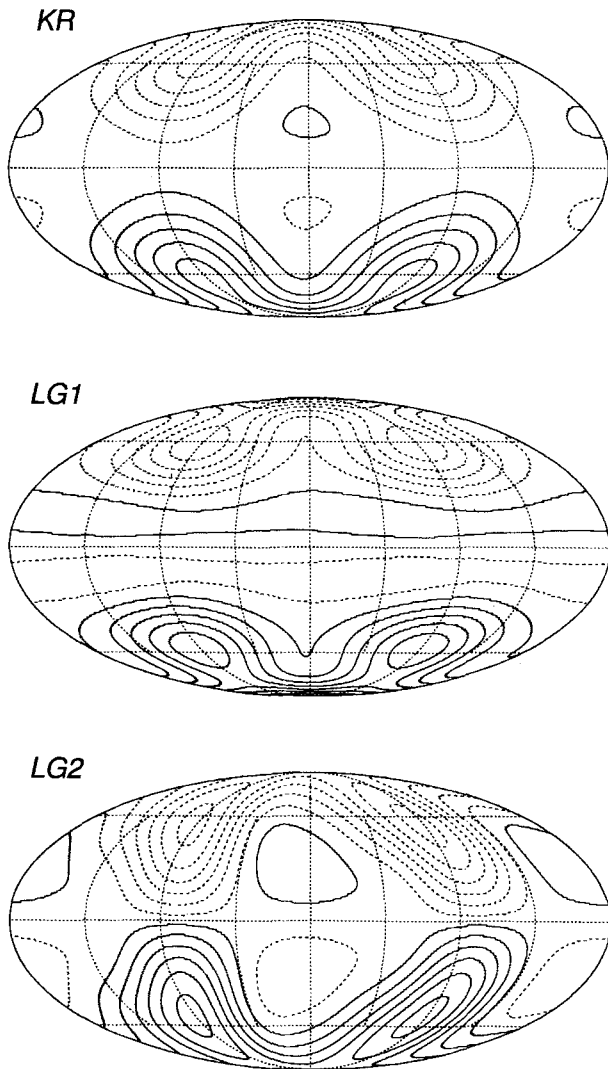


Figure 6. Surface magnetic fields for the three dynamo models with the field strength normalized so that the surface dipole is unity, $\|\mathbf{B}_{SD}\| = 1$. The contour intervals are all equal.

We suggest, however, that it is also possible that the spatial distribution of helicity plays a role in dynamo efficiency. In Fig. 7 we show plots of the spatial distribution of helicity. Although the ϕ -averaged helicity is not much different for each of the three models, other than in magnitude, the unaveraged plots show that the helicity of LG2 has a much simpler spatial distribution. In fact, for, say, the Northern Hemisphere, the velocity field of LG2 has a helicity which is predominantly of one sign, whilst both KR and LG1 have large regions where the helicity is of opposite sign. The simple helicity distribution of LG2 could have a role in making it an efficient dynamo, as an α -effect could be sustained easily by a simple distribution of helicity. On the other hand, for KR and LG1 the magnetic field is twisted in one region of helicity, but untwisted in the neighbouring region of opposite helicity, a complication which can only act to reduce the efficiency of the α -effect, thereby requiring larger magnetic Reynolds numbers.

Because of the formulation of our optimization procedure, there is a trade-off between the spatial complexity of the magnetic field, $\langle \nabla^2 \mathbf{B} \rangle$, and the magnetic Reynolds number,

R_m . Among the three dynamo models considered here, the dynamo with a redder spectrum has a larger R_m than the dynamo with a bluer spectrum. At first glance such a trade-off might appear to be counter-intuitive. Because advection tends to twist and tangle the magnetic field, whilst diffusion only acts to simplify its spatial form, it might be thought that a fluid motion which sustains spatially simple magnetic fields would possess a small R_m , and a fluid motion which sustains spatially complex magnetic fields would have a large R_m . However, this expectation is not borne out by the examples presented here.

An explanation for this may be due, in part, to differential rotation. In its simplest form, $\alpha\omega$ dynamo theory presumes that differential rotation acts on the poloidal dipole giving rise to the toroidal quadrupole. This same differential rotation, however, can act to assist diffusion in destroying higher-degree spatially complex components of the magnetic field, particularly the non-axisymmetric components. In Fig. 8 we show, schematically, differential rotation, \mathbf{t}_1^0 , acting on a simple loop of magnetic field. As we have drawn it, this could represent a non-axisymmetric poloidal magnetic field with an initial characteristic dimension D and diffusive time-scale $\tau_D = D^2/\eta$; after advective shearing, the magnetic loop is stretched and twisted so that its characteristic dimension is decreased to δ , where $\delta \ll D$, and with diffusive time-scale $\tau_\delta = \delta^2/\eta$. Since $\tau_\delta \ll \tau_D$, the magnetic field is destroyed more efficiently than if no differential rotation had existed. Obviously, for dynamo action, the poloidal field is constantly being regenerated via the α -effect, but if differential rotation is strong compared with the poloidal motion, as it is for our dynamos with large R_m , then the diffusive decay of the non-axisymmetric, high degree, i.e. spatially complex, components of the magnetic field is enhanced. This is a recipe for inefficiency, since by Cowling's theorem some non-axisymmetric components of the magnetic field must exist, and the only way of maintaining dynamo action, despite rotational enhancement of diffusion, is with larger magnetic Reynolds numbers.

6 DISCUSSION

Our optimization approach represents a systematic means of constructing dynamo models that are both mathematically tractable and physically reasonable. Although, for the purposes of illustration, we limited ourselves to a severely restricted class of fluid motions, there is nothing to prevent an extension of this technique to consider a much wider class of fluid motions, represented, say, by radial grid points and a high-degree spherical harmonic expansion. Such a treatment could yield kinematic models with convergence properties superior to those found here. The kinematic optimization method could be used to find those dynamos that minimize physically interesting quantities; for example, finding the dynamo with minimum magnetic Reynolds number or the dynamo with minimum ohmic dissipation. Such investigations would establish lower bounds on some interesting physical quantities relating to all dynamos, including, but not being limited to, the geodynamo.

An analogous and geophysically important inverse problem would involve finding the velocity fields that sustain core surface fields that are constrained to resemble the Earth's and that minimize some geophysically important quantity of the core: for example, optimizing for the kinematic dynamo, which

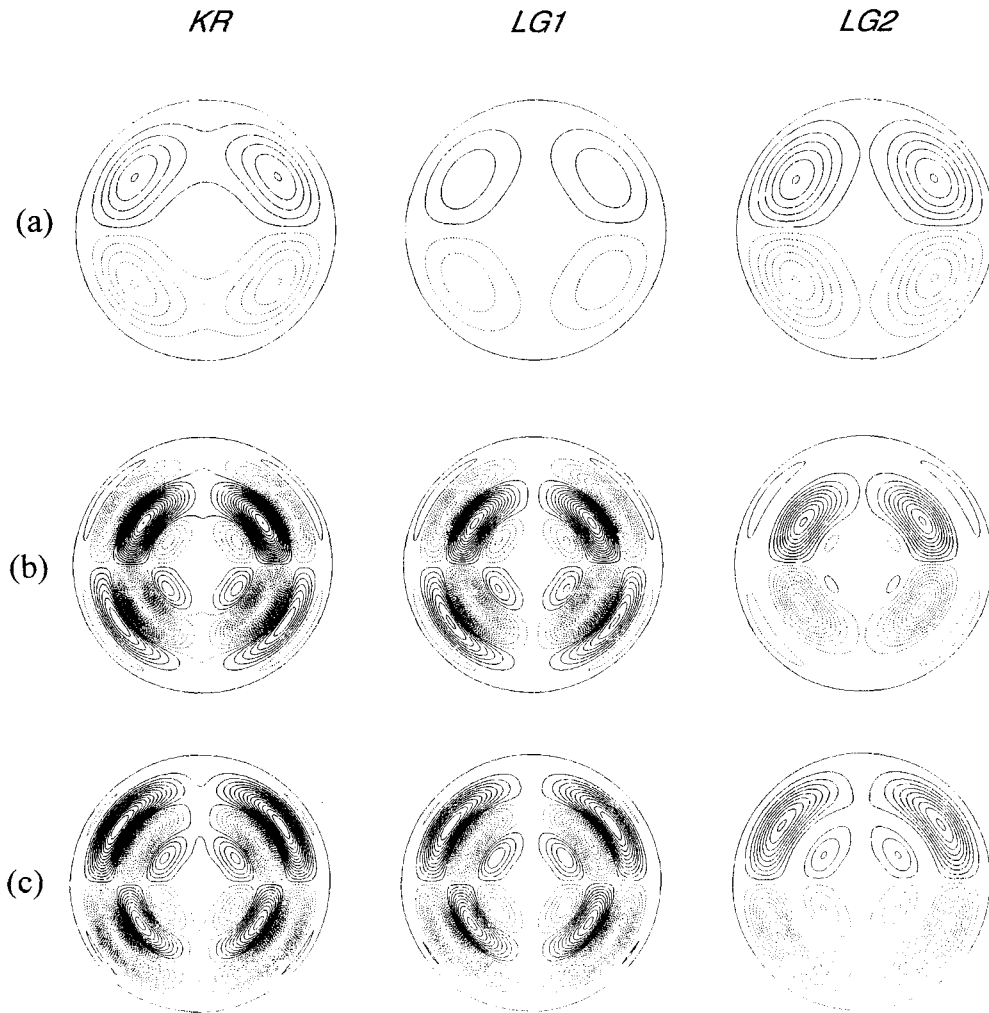


Figure 7. Helicity, $\mathbf{u} \cdot \nabla \times \mathbf{u}$, for the three dynamo models with unit normalization of the velocity field, $\langle \mathbf{u} \rangle = 1$. The contour intervals for KR and LG1 are equal and a tenth that for LG2. (a) Azimuthal average of the helicity in a meridian plane; (b) helicity in the meridian plane $\phi = 0^\circ$; (c) helicity in the meridian plane $\phi = 90^\circ$.

minimizes a weighted combination of misfit to the observed field and average internal field strength. Of course, we do not contend that the geodynamo operates in a regime that minimizes its average field strength, but by tying such an inversion directly to the observed magnetic field, or a suitable approximation of it, one could place a lower bound on the internal field strength, a quantity of obvious importance for understanding the dynamic effects of the Lorentz force. Alternatively, one could minimize a combination of misfit to the observed field and ohmic dissipation in the core, thereby placing a lower bound on the ohmic dissipation, a quantity which is currently poorly constrained but of central importance to core thermodynamics.

In principle, our optimization technique could also be extended to a dynamic analysis. Like the forward kinematic dynamo problem, the forward dynamic dynamo problem suffers from a degree of arbitrariness, although of a different type. For a forward dynamic analysis, instead of specifying the fluid motion, as one does for the kinematic case, one needs to specify the physical parameters of the fluid, the viscosity and thermal diffusivity for example, and, of course, the boundary

and initial conditions. Once this is done, the forward dynamic problem, like the forward kinematic problem, consists of a numerical experiment: do the specified physical properties allow the fluid to convect in such a way that dynamo action is sustained? This programme has been tried by a number of investigators (Gubbins 1975; Gilman 1983; Glatzmaier 1985; Zhang & Busse 1989; Glatzmaier & Roberts 1995), but the interpretable results are few in relation to the enormous effort expended.

In treating the dynamic dynamo as an optimization problem, one might solve for the extrinsic parameters, the Taylor, Chandrasekhar, Prandtl and Rayleigh numbers, by, for example, finding the set which optimizes numerical convergence. Alternatively, one could allow for lateral variation of temperature or heat flux on the core-mantle boundary, as done by Zhang & Gubbins (1993) for the forward, non-magnetic problem, and invert the observed magnetic field for the temperature or heat flux on the core surface. Clearly, an optimization approach to dynamo theory presents many possible inversions which could improve our understanding of the inner workings of the Earth's core and the geodynamo.

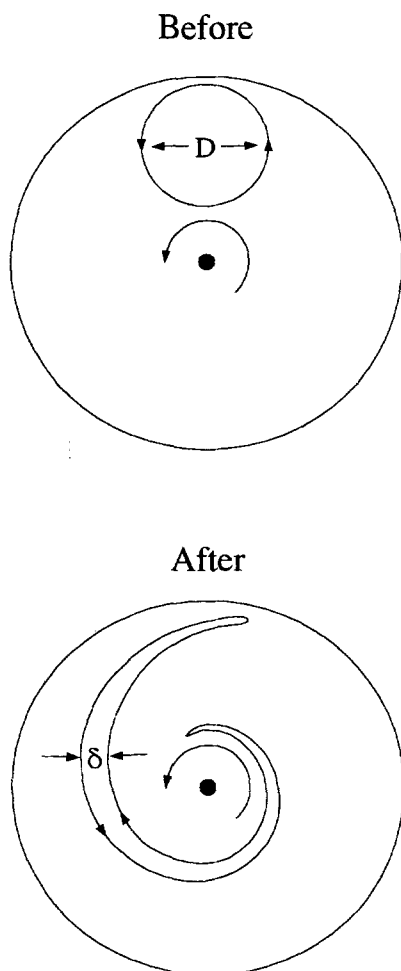


Figure 8. The effect of differential rotation on a non-axisymmetric, poloidal field line.

ACKNOWLEDGMENTS

This work was supported by NERC grant GR3/8238.

REFERENCES

- Bloxham, J. & Gubbins, D., 1985. The secular variation of the Earth's magnetic field, *Nature*, **317**, 777–781.
- Bloxham, J., Gubbins, D. & Jackson, A., 1989. Geomagnetic Secular Variation, *Phil. Trans. R. Soc. Lond.*, **329**, 415–502.
- Braginsky, S.I., 1964. Kinematic models of the earth's hydromagnetic dynamo, *Geomagnetism and Aeronomy*, **4**, 572–583, English translation.
- Bullard, E.C. & Gellman, H., 1954. Homogeneous dynamos and terrestrial magnetism, *Phil. Trans. R. Soc. Lond.* **247**, 213–278.
- Busse, F.H., 1983. Recent developments in the dynamo theory of planetary magnetism, *Ann. Rev. Earth planet. Sci.*, **11**, 241–268.
- Cowling, T.G., 1934. The magnetic field of sunspots, *Mon. Not. R. astr. Soc.*, **94**, 39–48.
- Dennis, J.E. & Schnabel, R.B., 1983. *Numerical methods for unconstrained optimization and nonlinear equations*, Prentice-Hall, New Jersey.
- Gibson, R.D. & Roberts, P.H., 1969. The Bullard and Gellman Dynamo, in *The Application of Modern Physics to the Earth*

- and *Planetary Interiors*, pp. 577–602, ed. Runcorn, S.K., Wiley Interscience, New York.
- Gilman, P.A., 1983. Dynamically consistent nonlinear dynamos driven by convection in a rotating spherical shell. II. Dynamos with cycles and strong feedbacks, *Astrophys. J. Suppl.*, **53**, 243–268.
- Glatzmaier, G.A., 1985. Numerical simulations of stellar convective dynamos III. At the base of the convection zone, *Geophys. astrophys. Fluid Dyn.*, **31**, 137–150.
- Glatzmaier, G.A. & Roberts, P.H., 1995. A three-dimensional convective dynamo solution with rotating and finitely conducting inner core and mantle, *Phys. Earth planet. Inter.*, **91**, 63–75.
- Gubbins, D., 1973. Numerical solutions of the kinematic dynamo problem, *Phil. Trans. R. Soc. Lond.*, **274**, 493–521.
- Gubbins, D., 1975. Numerical solutions of the hydromagnetic dynamo problem, *Geophys. J. R. astr. Soc.*, **42**, 295–305.
- Gubbins, D. & Bloxham, J., 1987. Morphology of the geomagnetic field and implications for the geodynamo, *Nature*, **325**, 509–511.
- Gubbins, D. & Kelly, P., 1993. Persistent patterns in the geomagnetic field during the last 2.5 Myr, *Nature*, **365**, 829–832.
- Gubbins, D. & Zhang, K., 1993. Symmetry properties of the dynamo equations for palaeomagnetism and geomagnetism, *Phys. Earth planet. Inter.*, **75**, 225–241.
- Gubbins, D., Masters, T.G. & Jacobs, J.A., 1979. Thermal evolution of the Earth's core, *Geophys. J. R. astr. Soc.*, **59**, 57–99.
- Hide, R. & Roberts, P.H., 1979. How strong is the magnetic field in the Earth's liquid core?, *Phys. Earth planet. Inter.*, **20**, 124–126.
- Hutchison, K.A., 1990. Geomagnetic field modelling, *PhD thesis*, University of Cambridge, Cambridge.
- Hutchison, K.A. & Gubbins, D., 1990. A model of the geomagnetic field for the 17th century, *J. geophys. Res.*, **95**, 10 769–10 781.
- Hutchison, K.A. & Gubbins, D., 1994. Kinematic magnetic field morphology at the core mantle boundary, *Geophys. J. Int.*, **116**, 304–320.
- Johnson, C.L. & Constable, C.G., 1995. The time-averaged geomagnetic field as recorded by lava flows over the past 5 Myr, *Geophys. J. Int.*, **122**, 489–519.
- Kumar, S. & Roberts, P.H., 1975. A three-dimensional kinematic dynamo, *Proc. R. Soc. Lond.*, **344**, 235–238.
- Lilley, F.E.M., 1970. On kinematic dynamos, *Proc. R. Soc. Lond.*, **316**, 153–167.
- Malvern, L.E., 1969. *Introduction to the mechanics of a continuous medium*, Prentice-Hall, New Jersey.
- Moffatt, H.K., 1978. *Magnetic Field Generation in Electrically Conducting Fluids*, Cambridge University Press, Cambridge.
- Nakajima, T. & Kono, M., 1991. Kinematic dynamos associated with large scale fluid motions, *Geophys. astrophys. Fluid Dyn.*, **60**, 177–209.
- Parker, E.N., 1955. Hydromagnetic Dynamo Models, *Astrophys. J.*, **122**, 293–314.
- Pekeris, C.L., Accad, Y. & Shkoller, B., 1973. Kinematic dynamos and the earth's magnetic field, *Phil. Trans. R. Soc. Lond.*, **275**, 425–461.
- Roberts, P.H., 1972. Kinematic dynamo models, *Phil. Trans. R. Soc. Lond.*, **272**, 663–698.
- Sclater, J.G., Jaupart, C. & Galson, D., 1980. The heat flow through oceans and continents, *Rev. Geophys. Space Phys.*, **18**, 269–311.
- Stacey, F.D., 1977. *Physics of the Earth*, John Wiley & Sons, New York.
- Steenbeck, M., Krause, F. & Rädler, K.-H., 1966. A calculation of the mean electromotive force in an electrically conducting fluid in turbulent motion, under the influence of Coriolis forces, *Z. Naturforsch.*, **21a**, 369–376.
- Zhang, K. & Gubbins, D., 1993. Convection in a rotating spherical fluid shell with an inhomogeneous temperature boundary condition at infinite Prandtl number, *J. Fluid Mech.*, **250**, 209–232.
- Zhang, K.K. & Busse, F.H., 1989. Convection driven magnetohydrodynamic dynamos in rotating spherical shells, *Geophys. astrophys. Fluid Dyn.*, **49**, 97–116.